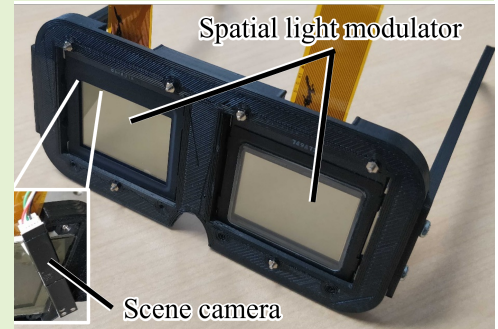


Smart Dimming Sunglasses for Photophobia Using Spatial Light Modulator

Xiaodan Hu, *Student Member, IEEE*, Yan Zhang, Naoya Isoyama, Hideaki Uchiyama, Nobuchika Sakata and Kiyoshi Kiyokawa, *Member, IEEE*

Abstract—We introduce a smart dimming sunglasses system designed for photophobia sufferers, particularly those highly sensitive to light intensity. The system incorporates a spatial light modulator (SLM) to filter light based on camera-detected scenes, controlling pixel transmittance via a modulation function for automated non-linear field of view dimming, thus offering flexible light modulation to meet the visual needs of photophobic users. However, a conventional occlusion mask on the SLM, aimed at blocking incoming light, appears blurred and insufficient due to a misaligned focal plane. Previous attempts to remedy this with an aperture-based expanded mask led to over-blocking (occlusion leak), due to an excessively large expansion radius. Our work, therefore, focuses on developing an optimization model that simulates a defocused occlusion mask and determines the degraded pixels' effective contribution by studying pixel transmittance occlusion efficiency. This optimized mask successfully attenuates bright areas to appropriate brightness levels without unnecessary attenuation of areas that do not require modulation, overcoming the limitations of both the unprocessed and aperture-based expanded masks.

Index Terms—Augmented reality, Human augmentation, Optical control, Smart glasses



I. INTRODUCTION

Photophobia, or light sensitivity, is a common symptom of various ophthalmic and neurologic conditions, causing discomfort, headaches, or other unpleasant feelings under intense light [5], [15], [21]. This symptom can also be triggered by other factors such as the flicker of fluorescent lights or wavelength-specific light [8], [20], [26]. However, our study mainly concentrates on photophobia symptoms incited by high light intensity, exemplified by conditions like autism spectrum disorder (ASD) [4], [7]. ASD-related photophobia stems from neurodevelopmental abnormalities, leading to larger static baseline pupil sizes or abnormal pupillary responses, and consequently, a brighter field of view [1], [7].

While traditional eyewear like dark sunglasses or tinted lenses provide relief from photophobia [6], they can exacerbate the dark adaptation, leading to heightened sensitivity [18].

This work has been submitted to the IEEE for possible publication. Copyright may be transferred without notice, after which this version may no longer be accessible.

This work was supported by JSPS KAKENHI 22H00539 and JST SPRING Grant Number JPMJSP2140, Japan.

X.H., H.U. and K.K. are with Nara Institute of Science and Technology (NAIST), Ikoma, Nara 6300192, Japan (e-mail: hu.xiaodan.ht1, hideaki.uchiyama, kiyo@is.naist.jp).

Y.Z. was with NAIST. He is now with Shanghai Jiao Tong University, Shanghai 200240, China (e-mail: yan-zh@sjtu.edu.cn).

N.I. was with NAIST. He is now with Otsuma Women's University, Chiyoda, Tokyo 1028357, Japan (e-mail: isoyama@otsuma.ac.jp).

N.S. was with NAIST. He is now with Ryukoku University, Otsu, Shiga 5202194, Japan (e-mail: sakata@rins.ryukoku.ac.jp).

Alternatives such as auto-dimming glasses [24] that enable a fast tint changing with a light sensor can address the problem of dark adaptation. Nevertheless, the linear global dimming method is not suitable for high-contrast environments. Since photophobic people are even sensitive to fluorescent lights at night, auto-dimming eyeglasses are not the best choice for everyday wear.

Inspired by the potential of augmented reality (AR) technology as an assistance for eye conditions [2], [10], [11], [23], we enhance the concept of a system using a spatial light modulator (SLM) for selective dimming and a scene camera for scene detection [12]–[14], [16], [19], [22]. Our system employs an occlusion mask, formed by pixels with low transmittance on the SLM, to filter incoming light. This occlusion mask is computed based on the image intensity captured by the scene camera.

However, through geometric optics, it is known that an aperture-sized mask must be formed to adequately block a point in the distance [14], [22]. Otherwise, the occlusion mask becomes out-of-focus and significantly blurred because the SLM is not in the same focal plane as the real scene, resulting in incomplete occlusion. If the occlusion mask is expanded by the aperture radius, it becomes too large, leading to occlusion leak [14]. In this scenario, the mask tends to fully block not only the target pixel, but also the surrounding area, thereby attenuating a larger region than required.

In this paper, we further refine the SLM control method for balancing the observation contrast. To address the issue

of defocused occlusion mask, we propose an optimization method tailored to the smart dimming sunglasses system and photophobic users. The visual results effectively demonstrate the efficiency of the control method (Fig. 9).

Our main contributions include the following:

- A compact architecture of smart sunglasses for photophobia.
- A control method for SLM to balance the contrast of observation using only the image intensity captured by a camera.
- An optimization method that provides sufficient dimming with a defocused blurred occlusion mask.

II. RELATED WORK

In this section, we examine currently available glasses for photophobia, and offer a brief overview of the application of AR and adaptive optics (AO) in various ocular disorders. Furthermore, we explore some influential AR and computational imaging technologies that have inspired our work.

A. Glasses for Photophobia

Colored glasses, particularly those with blue lenses, have been shown to effectively alleviate photophobia symptoms [6]. However, these glasses impart their lens color onto the entire field of view, leading to another potential source of discomfort. Moreover, it is often medically advised against wearing dark or colored glasses indoors, as patients may become dark-adapted and consequently experience increased light sensitivity [15].

Auto-dimming glasses, used in sports and lifestyle applications, adjust lens transmittance based on the intensity of ambient light, especially sunlight [24]. However, these globally dimming sunglasses are not suited for certain complex environments, such as those with high-contrast interior lighting or nighttime illumination.

Our proposed smart dimming sunglasses adjust the light intensity of the user's field of view in a nonlinear, real-time manner. The adjustments are guided by a high dynamic range (HDR) camera, which detects real scenes, and are determined according to predefined user dimming requirements, thereby ensuring a more comfortable visual experience for the user.

B. AR and AO Assistant devices for Ophthalmic Diseases

Vision impairment is a global issue affecting at least 2.2 billion individuals, many of whom cannot correct their vision disorders with conventional glasses [28]. With the advent of advancements in AR and AO, there has been a surge in research aimed at developing solutions for these visual impairments [2], [3], [10], [11], [17], [23].

A case in point is the development of autofocus glasses for presbyopia, a common age-related condition that hampers close-up vision. Standard presbyopic glasses allow individuals to see objects only at a fixed distance. In response to this, Hasan *et al.* designed a lightweight autofocusing smart eyeglass with a distance sensor and tunable eyepieces for dynamic calculation of optical power and focus adjustment [10], [11].

Furthering this technology, Padmanaman *et al.* incorporated an eye-tracker and depth camera to control tunable lenses, culminating in the development of the "autofocals" system, a promising future solution for presbyopia assistance [23].

Another widespread issue is cataracts, characterized by an opaque area in the crystalline lens and a common cause of preventable blindness. Arias *et al.* proposed an optical correction system for cataracts, which implements a wavefront shaping technique to focus light through a scattering medium like a cataractous lens [2]. The system uses a liquid crystal device on silicon SLM to reproduce and correct various degrees of cataracts. However, the final image contrast remained inadequate. They suggested that their system could be enhanced by combining it with an AR setup to boost contrast.

Drawing inspiration from AR and AO devices, we develop smart dimming sunglasses that use a transmissive SLM to modulate light intensity. This solution can aid individuals with incurable photophobia symptoms, such as those associated with neurodevelopmental disorders.

C. High Dynamic Range Imaging Using Spatial Light Modulator

Nayar and Branzoi introduced an adaptive dynamic range camera based on an SLM [22]. In their system, a transmissive liquid crystal display (LCD) is situated in front of a standard camera. The transmittance of corresponding pixels on the LCD panel is adaptively adjusted to modify the exposure of the image detector's pixels. Nevertheless, because the observer in our system is the human eye, this adaptive correction approach via digital image data capture is not directly applicable to eyewear.

Echoing the concept of programmable dynamic range imaging, Wetzstein *et al.* proposed proof-of-concept prototypes [27]. They used an SLM to spatially filter incoming light, demonstrating manipulable optical contrast modulation in perceptually-motivated applications. They developed two devices: a focused scope-like device and a defocused window-like device. For the purpose of creating lightweight dimming sunglasses, we adopt a design akin to their defocused window-like device. However, they provided limited information about this device, and seemed to consider the blur caused by out-of-focus as unnecessary for correction.

In our experiments, defocused blur results in significant occluding incompleteness, a critical issue for individuals with photophobia. Consequently, addressing this issue of out-of-focus blur is a primary objective of our research.

D. Occlusion-capable AR Displays

In recent years, occlusion-capable AR displays [14], [16], [19] have been developed, which can dim bright spot in the user's vision. The image-forming occlusion mask created on an SLM between the real scene and the virtual object efficiently blocks the incident light, resulting in a more vivid virtual object. However, in order to achieve per-pixel occlusion without optical blur of the occlusion mask, additional optics must be incorporated into the optical path. In the ELMO-4 AR display [16], mutual occlusion is realized by four

convex lenses, two prisms, and three mirrors. These large numbers of optics and long optical paths make the head-mounted display (HMD) bulky and costly. Meanwhile, the extensive use of lenses results in a narrow field of view (FOV). Although a wide-view occlusion-capable AR display with a FOV of $H114^\circ \times 95^\circ$ was recently developed [29], [30], the sophisticated optical design made the HMD substantially bulkier.

This technique of precise per-pixel control by optical lenses is commonly referred to as "hard-edge occlusion," whereas the utilization of defocused occlusion through transmissive SLMs is known as "soft-edge occlusion." Soft-edge occlusion implemented with transmissive SLMs provides several advantages over conventional optical see-through head-mounted displays (OST-HMDs). These advantages include a reduction in the overall system size, a wider FOV, and minimized distortion. However, a significant challenge with soft-edge occlusion is that it lacks optical components for achieving proper focus. Consequently, when the human eye focuses on a specific distance, the occlusion mask displayed in front of the eye is positioned outside the focal plane, resulting in blurring of the mask and incomplete blocking of the intended area.

Maimone *et al.* [19] proposed computational AR eyeglasses based on a set of backlit stacked LCD panels to achieve a compact and wide FOV AR display. Such multi-layer structure achieved nearly per-pixel occlusion by attenuating the intensity layer by layer. Although this approach improved the issue of blurred occlusion mask, it also resulted in reduced transmittance and increased thickness of the optical system due to the multi-layer LCD setup. Hiroi *et al.* [12] conducted research on modulating light entering the eyes using occlusion on a single transparent LCD and overlaying virtual images from an OST-HMD to enhance underexposed regions. Later, their team [14] addressed the issue of incomplete occlusion caused by defocused masks by expanding the mask using an aperture or pupil radius as the expansion radius through geometric optics calculations. However, this approach resulted in oversized masks, leading to the phenomenon of "occlusion leak," where not only the target pixel but also the surrounding area was masked. To mitigate occlusion leak, they utilized an OST-HMD to generate both a virtual background and a virtual object that covered the entire occlusion mask, effectively eliminating the artifacts caused by occlusion leak.

In this paper, we also use the transparent LCD to manufacture smart dimming glasses. Unlike virtual display-based systems, we address the issue of occlusion leak by employing weighted optimization to determine the optimal expansion radius. This allows us to achieve effective occlusion without occlusion leak.

III. SYSTEM ARCHITECTURE AND METHOD

We made the decision to avoid the use of additional optical lenses, which would have extended the optical path and restricted the FOV. Instead, we opted for a single SLM for efficient reduction of dazzle and to achieve compact sunglasses. However, the absence of optical lenses for focusing light rays creates a challenge in achieving simultaneous focus between

the LCD panel and the object space, leading to blurring of the occlusion mask due to being out-of-focus. In Section III-C, we present an occlusion mask optimization approach that ensures the blurred mask still offers adequate occlusion.

A. Benchtop Prototype Designs

We first built a benchtop prototype (Fig. 1(bottom left)) to test and evaluate the system. The benchtop prototype is composed of two parts; a light modulation part and an illuminance detection part (Fig. 1(right)). The former consists of a primary SLM, in particular, a transmissive LCD, which displays an occlusion pattern for a human eye, and the latter consists of a scene camera (SC) and a secondary LCD with uniform transmittance that are positioned just above the primary LCD to minimize the parallax. Both LCDs work with a polarizer. Note that we avoid introducing the beam splitter to share the same viewpoint, but directly place the two cameras at a close position in order to maximize the FOV. As the incident light becomes polarized, the amount of light received by the image sensor is reduced. In addition, some slight diffraction is generated from the gap of the liquid crystal element. Thus the secondary LCD guarantees that the SC captures similar images as the human eye through the primary LCD without pattern dimming. In the prototype system we built, an eye-simulating camera (EC) is placed at the position of the human eye. We also designed the wearable prototype (Fig. 1(top left)). The LCDs are utilized directly as the lens due to the simple structure, and the scene camera can be put behind the one of an LCD.

Fig. 1(right) shows the process flow with pictures illustrating images taken by the SC and the EC. The real environment is first captured by the SC through the secondary LCD with uniform transmittance. Then, an appropriate occlusion mask is computed and displayed on the primary LCD for the EC so that the EC captures images with a more balanced contrast.

B. Photometry and Radiometry

Before introducing the occlusion algorithm, we first describe the definitions and relationship between photometry and radiometry. Since we quantify the human visual system in terms of camera systems, we next describe the perceptual process of the human visual system in photometric terms and the imaging process of the corresponding camera system in radiometric terms.

Humans can perceive brightness due to the light that passes through the pupil, crystalline lens, and finally stimulates the photoreceptor cells in the retina. Similarly, the camera is able to image because the light enters through the aperture, optical lens, and eventually hits the image sensor, which converts the light signal into an electrical signal.

As depicted in Fig. 2(b), when light passes through an SLM, the original radiance L is attenuated to L' according to the transmittance T of the SLM:

$$L' = TL.$$

For the camera system, the exposure time linearly affects the radiance received by the image sensor, which converts

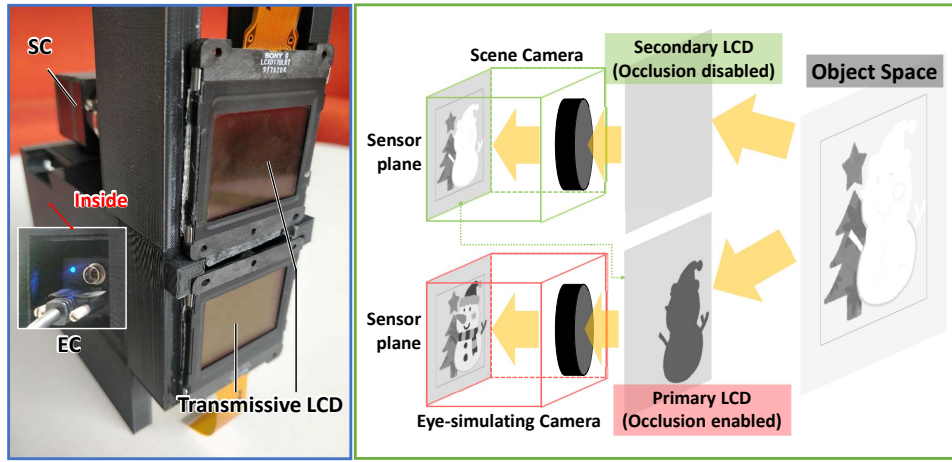


Fig. 1. (left) Benchtop prototype for experimentation and evaluation. (right) Process flow of the benchtop prototype. The real environment is first captured by the SC through the secondary LCD with uniform transmittance. Then, an appropriate occlusion mask is computed according to the images captured by SC and displayed on the primary LCD for the eye-simulating camera (EC) so that the EC observes the scene with a more balanced contrast (on the sensor plane of EC).

the sensor irradiance into an electrical signal and further into a digital signal through an analog-to-digital converter. We assume that the attenuated radiance L' , which is equivalent to the perceived luminance by the human eye, is linearly related to the sensor irradiance or retina illuminance. Consequently, the captured pixel intensity can be expressed as a non-linear mapping of the attenuated radiance:

$$I_{EC} = f_r(L') = f_r(TL), I_{SC} = f_r(T_{max}L), \quad (1)$$

where I_{EC} and I_{SC} represent the pixel intensity captured by the EC and the SC, respectively. The secondary LCD provides uniform dimming, and its transmittance can be approximated as a constant value T_{max} . The response function f_r can be determined through measurements with a luminance meter.

The transmittance of the LCD is related to the applied voltage, however, the voltage in each crystal liquid element is inaccessible, while the pixel intensity on the LCD is more intuitive and easily obtainable. Therefore, we quantify the transmittance T with a certain grayscale value I_m on the LCD by placing a luminance meter after the LCD to measure the attenuated luminance, which is shown in Fig. 3(a) (This measurement result depends on the devices, we give the detailed configuration in Section IV-A). The relationship can be fitted by a sigmoid function f_s as:

$$T = f_s(I_m). \quad (2)$$

C. Occlusion Algorithm

In this section, we propose the overall occlusion algorithm based on quantification and measurement of the camera system. In Section III-C.1, we give the modulation method for attenuating the brightness. In Section III-C.2, we address the challenge of the blurry mask due to out-of-focus and use the point spread function to simulate the out-of-focus process. Finally, we describe the proposed optimization approach for the occlusion mask in Section III-C.3.

1) Modulation Function: As observed from the system configuration, the only input in the occlusion algorithm is the image intensity I_{SC} converted from the sensor irradiance captured by SC. We define the target image intensity on EC, which represents the brightness perceived by the human eye, as I_t . Referring to Equation 1, this can be expressed as:

$$I_t = f_r(T_t L), \quad (3)$$

Here, T_t denotes the target transmittance of the LCD, aiming to achieve the desired image intensity I_t on EC.

Based on the target image intensity I_t , the attenuation ratio a_t is defined as:

$$a_t = \frac{I_t}{I_{SC}}, \quad (4)$$

This can be interpreted as the ratio between the image intensity before modulation (I_{SC}) and the intensity after modulation (I_t).

Fig. 3(b) illustrates the modulation functions, with the dashed and dash-dot lines representing the mapping without modulation and under linear modulation, respectively. In both cases, the modulations are uniform, reducing each pixel intensity by a fixed attenuation ratio.

To address the symptoms of atypical vision in individuals with photophobia without introducing additional visual disturbances, we define the desired modulation effect as follows. While there are various strategies for computing the occlusion mask, a smooth visual experience can be achieved by satisfying the following requirements:

- High-intensity regions should be dimmed for comfortable viewing, while remaining discernible,
- Low-intensity regions should not be dimmed significantly and should be preserved as much as possible,
- Regions with higher (lower) intensity should appear brighter (darker) after modulation.

These requirements are reflected in the properties of the proposed modulation function, which should:

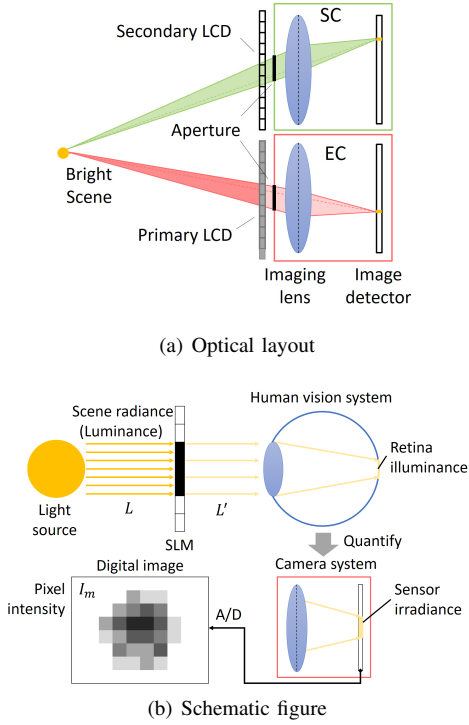


Fig. 2. Optical layout and schematic figure of the proposed system. (a) Two mappings, the one from the primary LCD (pattern dimming) to the image detector of the eye camera (EC), and the other from the image detector of the scene camera (SC) to the EC, are both given by a homography. (b) The scene radiance L is attenuated by the SLM to L' , and shines into the user's eye. To optimize and evaluate the system, the camera receives the attenuated radiance L' as sensor irradiance, and finally converts to the digital signal with pixel intensity I_m .

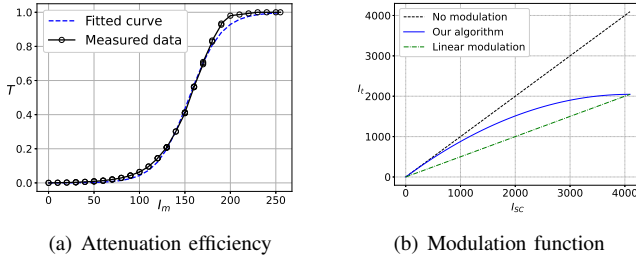


Fig. 3. (a) The relationship between the transmittance (T) of the LCD we use and the pixel intensity (I_m) of the occlusion mask can be fitted by a sigmoid function. (b) Modulation functions between original (I_{SC}) and target (I_t) pixel intensities; no modulation (dashed), linear modulation (dash-dot), and parabolic modulation (solid).

- Intersect with the linear-modulation function at the highest intensity,
- Be tangent to the no-modulation function at the lowest intensity,
- Increase monotonically.

In practice, we have found that a parabolic curve, as shown in Fig. 3(b), satisfies these requirements. Therefore, given a target image intensity I_t , which can be adjusted according to the individual's light sensitivity, the necessary transmittance T_t of the LCD panel can be determined using Equations 1, 3, and 4. The corresponding pixel intensity I_m on the occlusion mask can be easily calculated using the inverse function of

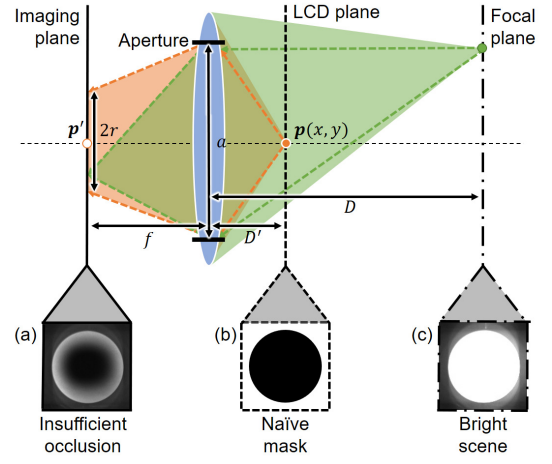


Fig. 4. The imaging process of the proposed system. While the LCD panel is not in the focal plane, a pixel p on the LCD plane can be imaged as a blurred disc with p' as the center and r as the radius. With the real bright scene (c), the computed naïve occlusion mask (b) is observed as an insufficient occlusion (a) that allows incoming light from the edge to penetrate the occlusion mask to induce stimuli.

Equation 2:

$$I_m = f_s^{-1}(T_t). \quad (5)$$

2) Out-of-focus Point Spread Function: It is known that in practice, when the user's focus is on a distant scene, the occlusion on the near LCD panel becomes blurred. For each pixel on the LCD, such blurred image created by imaging a point is commonly known as the out-of-focus point spread function (PSF) [9]. The schematic diagram that describes the out-of-focus PSF is shown in Fig. 4.

On the focal plane, points are imaged in focus, whereas the pixels on the LCD that are not on the focal plane are imaged as a blurred disc. For instance, a pixel p can be imaged as a blurred disc with p' as the center and r as the radius. If we assume that the imaging system adheres to a linear space-invariant imaging model, the image acquisition process—disregarding noise and diffraction aberrations—can be expressed as:

$$I_{EC}(x, y) = I_m(x, y) \otimes H_{OOF}(x, y), \quad (6)$$

Here, H_{OOF} represents the PSF of the imaging system and \otimes stands for a convolution operator. Assuming a circular aperture and an LCD plane roughly perpendicular to the optical axis of the lens, under severe defocus approximation, the PSF can be given by the geometrical projection:

$$H_{OOF}(x, y) = \frac{1}{\pi r^2} \text{circ}\left(\frac{\sqrt{x^2 + y^2}}{r}\right). \quad (7)$$

The radius r of the blurred disc can be calculated using the triangle ratio:

$$r = \frac{a}{2} \left| 1 - \frac{D'}{D} \right|, \quad (8)$$

Here, a refers to the diameter of the aperture, while D and D' are the depths of the focal plane and the LCD plane,

respectively. Generally, $D' \ll D$, allowing Equation 8 to be simplified to $r \approx a/2$.

As shown in Fig. 4, the circular occlusion mask (Fig. 4(b)) is computed from the bright scene (Fig. 4(c)) detected by SC. Following a PSF, EC observes a blurred occlusion mask (Fig. 4(a)) that is blurred at the edge and leads into insufficient occlusion.

3) Optimization for the Occlusion Mask: To address the problem of insufficient occlusion, previous works [22] expanded the mask by the aperture radius, at the same time, however, this approach also causes the problem of *occlusion leak* [14]. Itoh *et al.* offered a compensating method that overlay a video see-through video image onto the expanded occlusion mask to tackle this problem [14], however this method is clearly ineffective for our optical see-through system.

To summarize, it means that occluding with the original mask results in insufficient occlusion, and expanding by aperture radius results in occlusion leak because it aims to occlude completely. Therefore, it is necessary to optimize a suitable expansion radius to make the mask filter the right amount of light without causing occlusion leak.

Here, we construct a mathematical model with an optimization objective that is to allow the central pixel whose pixel intensity is not excessively degraded to form an *effective occlusion* as much as possible, and not to allow these pixels to leak out.

In the Equation 5 we described how the scene brightness I_{SC} determines the intensity of the pixels I_m displayed on the LCD panel. Let us consider an extreme case, i.e., an approximate binarized image as shown in Fig. 4(c) as the scene, where only the bright region in the middle exists with the dark region around it. Then the corresponding occlusion mask that should be displayed on the LCD is also binarized, as shown in Fig. 4(b).

The bright region \mathbb{B} and the dark region \mathbb{D} defined by the image captured by the SC (a schematic diagram is shown in Fig. 5(a)) can be defined as follows:

$$\mathbb{B} = \{(x, y) | I_{SC}(x, y) \geq t_b\}, \mathbb{D} = \overline{\mathbb{B}}, \quad (9)$$

where t_b is a threshold for defining the bright region and (\cdot) denotes the complement of a set. Therefore, the *effective occlusion* is the intersection of pixels whose pixel intensities are not excessively degraded with the bright region (shown as Fig. 5(b)), that is,

$$\mathbb{B}_e = \{(x, y) | I_{EC}(x, y) \leq t_e(x, y)\} \cap \mathbb{B} \quad (10)$$

where t_e is the threshold to determine whether the pixel is capable of sufficient light blocking, which should be inversely proportional to the derivative of the response curve in Fig. 3(a) as follows:

$$t_e(x, y) \propto \left(\frac{df_s}{dI_m(x, y)} \right)^{-1}. \quad (11)$$

On the contrary, the blurred occlusion (shown as Fig. 5(b)) is given as:

$$\mathbb{B}_b = \{(x, y) | I_{EC}(x, y) > t_e(x, y)\} \cap \mathbb{B}. \quad (12)$$

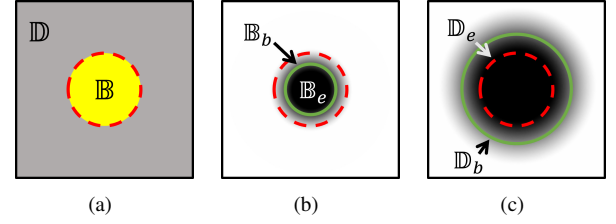


Fig. 5. Visualization of Equation 9-14. (a) Schematic diagram captured by the scene camera. The bright area is the part inside the red dashed circle which is represented as the set \mathbb{B} , the outside darker part is the set \mathbb{D} . (b) Schematic diagram captured by the eye-simulating camera when the mask cannot provide sufficient occlusion. The green solid line is to separate the *effective* occlusion and blurred occlusion. Inside the green solid circle is the set \mathbb{B}_e , and \mathbb{B}_b is the annulus between the red dashed circle and the green solid circle. (c) Schematic diagram captured by the eye-simulating camera when the mask is excessively large and leads to occlusion leak. Set \mathbb{D}_e is the annulus between the green solid circle and the red dashed circle, and the blurred occlusion outside the green solid circle is the set \mathbb{D}_b .

Similarly, when the effective occlusion leaks to the dark region, this area (shown as Fig. 5(c)) can be represented as follows:

$$\mathbb{D}_e = \{(x, y) | I_{EC}(x, y) \leq t_e(x, y)\} \cap \mathbb{D}. \quad (13)$$

And finally, when the blurred occlusion leaks to the dark region (shown as Fig. 5(c)), it can be given as:

$$\mathbb{D}_b = \{(x, y) | I_{EC}(x, y) > t_e(x, y)\} \cap \mathbb{D}. \quad (14)$$

Note that the set \mathbb{B} and the set \mathbb{D} are determined by the scene, i.e. \mathbb{B} and \mathbb{D} are fixed values, since the object we study is a static image. While I_{EC} is the image observed by the eye-simulating camera, if the occlusion mask is processed, I_{EC} will also be changed at the same time. Here we only explore the effect of expansion, and we introduce the superscript α on \mathbb{B}_e , i.e. \mathbb{B}_e^α , to denote the state of \mathbb{B}_e when the expansion radius is α . This expansion process is actually a morphological transformation, represented as:

$$I'_m(\alpha) = \min_{-\alpha < m, n < \alpha} I_m(x + m, y + n), \quad (15)$$

where I'_m is denoted as the expanded occlusion mask.

The optimization objective can then be interpreted as making the amount of pixels in \mathbb{B}_e as high as possible and trying to avoid the pixels in \mathbb{D}_e . Note that pixels in \mathbb{B}_b can exist; however, their weight of existence or avoidance increases as they approach or move away from the threshold t_e . Pixels in \mathbb{D}_b follow a similar rule. In this case, combined with Equation 9-15 the optimization problem can be represented as follows:

$$\begin{aligned} \max_{\alpha} \quad & S(\alpha) = \sum_{(x, y) \in \mathbb{B}_e^\alpha} \sigma_1 + \sum_{(x, y) \in \mathbb{B}_b^\alpha} \sigma_2 \cdot (1 - 2f_s(I_{EC}(x, y))) \\ & - \sum_{(x, y) \in \mathbb{D}_e^\alpha} \sigma_3 - \sum_{(x, y) \in \mathbb{D}_b^\alpha} \sigma_4 \cdot f_s(I_{EC}(x, y)), \\ \text{s.t.} \quad & \alpha \in \mathbb{Z}^+, \end{aligned} \quad (16)$$

where $\sigma_1 \sim \sigma_4$ are the weights for each pixel in the corresponding occlusion set, \mathbb{Z}^+ denotes the positive integers set.

According to the contribution level of each occlusion set, the contribution level of \mathbb{B}_e should be the highest so the weight should be set to the maximum, while the contribution or penalty level of the other three occlusion sets can be considered equal. In practice, we find σ_1 should be set large enough, otherwise Equation 16 will have no extreme value point. A unique extreme point will emerge in Equation 16 when σ_1 is at least three times larger than $\sigma_2 \sim \sigma_4$, as demonstrated in Fig. 7(b).

Since α represents discrete points, $S(\alpha)$ cannot be derived. However, the discrete optimization problem is relatively simple, and the maximum value of $S(\alpha)$ can be found via brute force search within a reasonable range.

IV. IMPLEMENTATION

In this section, we describe the entire system implementation, including the hardware and software setup and system calibration.

A. Hardware and Software Setup

As shown in Fig. 1(bottom left), the prototype system was developed by using two identical monochrome cameras with a SONY IMX 287 sensor (720×540 pixels, 12-bit depth) and a lens with the focal length of 6mm, f/1.6. The aperture is approximately equal to the large baseline pupil diameter as 3.8mm [1]. The two cameras are placed parallel to each other on the same vertical line, the distance D from the focal plane of both SC and EC is 2 meters. Both cameras are connected by a USB 3.0 link and transmit video data in real-time in a multi-threaded manner via a software development kit provided by the camera manufacturer. To avoid reflecting on the hardware, we covered the whole system with a piece of a black curtain. We used two sets of a SONY LCX017 panel (1024×768 pixels, 36.9×27.6mm active area, 705 dpi, 60 Hz, monochrome) and a pasted linear polarizer as the primary and the secondary LCDs. The transmittance of the LCD panel after power-on is 21%, and 10% with the pasted linear polarizer. The distances from both cameras to the corresponding LCD panel $D' = 10mm$. The LCD panels are controlled by an externally housed driver board connected by a VGA link to a PC with an AMD 8 cores 3.8GHz CPU and an NVIDIA GTX Titan X GPU. The 3D printed plastic framework of the prototype is designed in Autodesk®Fusion 360 and printed by ANYCUBIC. The system calibration and image processing procedures were based on OpenCV-Python, the entire software was written in Python 3.8.

B. System Calibration

1) *Calibration between the EC and the primary LCD*: As illustrated in Fig. 2(a), the mapping from the LCD plane to the image detector plane can be identified as a perspective one, implying that the mapping is dictated by a homography. We adjusted the focus of the EC alternately between the

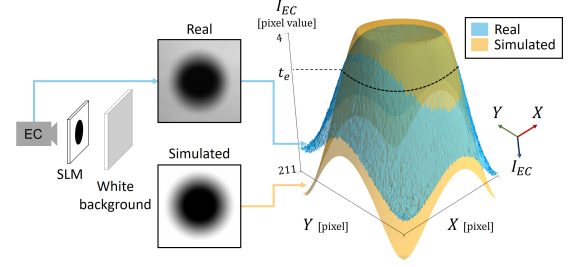


Fig. 6. (Left) The real occlusion is captured by the EC by placing a white background in front of the SLM. (Middle) Result of the out-of-focus simulated occlusion mask, and (Right) the 3-D visualization comparison with the real one.

focal plane and the LCD plane, recording the coordinates of the same projection on both planes. Following this, we employed library functions within OpenCV-Python to compute the homography matrix.

2) *Calibration between the EC and the SC*: Similarly, as illustrated in Fig. 2(a), the mapping from the SC to the EC is governed by a 2D homography matrix. In practice, we allowed the SC and EC to capture an image of an A1 size chessboard positioned on the focal plane, then calculated the homography matrix using library functions within OpenCV-Python.

V. EXPERIMENTS AND RESULTS

In this section, we demonstrate the occlusion optimization method using our proof-of-concept system. Section V-A introduces the procedure for out-of-focus PSF simulation via 2-D convolution. Section V-B presents experimental results with the naive mask, aperture-based expansion mask, and our proposed optimal masks. Finally, Section V-C evaluates and visualizes the performance of the proposed methods in cases of calibration deviation.

A. Out-of-focus PSF Simulation

As demonstrated in Fig. 6, to extract the real defocused occlusion mask, we first display a static occlusion mask in the shape of a circle (with a radius of 100 pixels) on the primary LCD. In order to capture as pure an occlusion mask as possible, the EC records the real occlusion mask while a white background is positioned in front of the benchtop system. We then subtract the background to extract the pure circle mask. Based on Equations 6 and 7, we can simplify this problem to:

$$\arg \min_r \|I_m \otimes H_{OOF}(r) - I_{EC}\|_2,$$

where the Euclidean distance is used to compute the similarity. To eliminate the effects of noise and diffraction aberrations from the edge pixels, we restrict the effective calculation area to the central part of the circle mask. The simulated occlusion mask does not need to perfectly match the real mask, which may be distorted due to noise or diffraction. Furthermore, since the primary purpose of the simulated mask is to serve as an evaluation criterion, we consider the *effective* occlusion area of the simulated mask. The final simulated mask should ensure that its *effective* occlusion area aligns with that of the real mask, as shown in Fig. 6(right). The areas of the real and

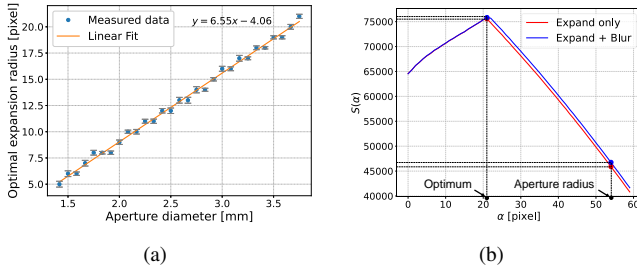


Fig. 7. (a) A mapping relationship between the optimal expansion radius and the aperture diameter allows the system to perform an optimized mask from the user's pupil size. (b) The image of Equation 16 with optimum at $\alpha = 21$. According to our optimization model, the function $S(\alpha)$ calculated using the aperture radius is significantly lower than the one calculated using the optimum radius. The blue curve represents $S(\alpha)$ when an additional blurring process is applied. Although the optimal $S(\alpha)$ with additional blurring is larger than that of a simple expansion, the difference is not significant.

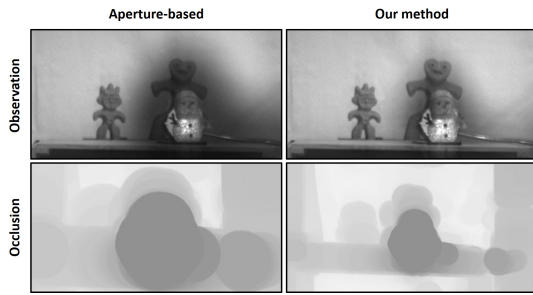


Fig. 8. Occlusion leak visualization. By displaying a static occlusion mask on the LCD, the occlusion leak is made evident when the background is replaced with a light color.

simulated 3-D figures that are within t_e are essentially the same.

B. Optimization Method

Upon confirming the PSF for out-of-focus simulation convolution, in accordance with the process outlined in Section III-C.3, we compared our methods with the naive mask and the aperture-based expansion mask in high-contrast environments. The aperture-based expansion radius α_a at the pixel level can be easily calculated from the size and resolution of the LCD panel as follows:

$$\alpha_a = \frac{a}{2} \cdot \frac{36.9}{1024} \approx 53,$$

while the optimal expansion radius of our method is $\alpha = 21$. There exists a mapping relationship between the optimal expansion radius and the aperture diameter, as demonstrated in Fig. 7(a). In this experiment, we fixed the aperture size to 3.8 mm [1] and adjusted the exposure to simulate the photophobic vision effect. The results are shown in Fig. 9.

To assess our method's capacity to handle occlusion leak, we illuminated a translucent snowman doll with an incandescent bulb positioned behind it. Two clay statues behind the bulb were only lit by ambient room light. Since the naive mask is blurred due to out-of-focus and the defocused mask produced by simulation does not provide sufficient blocking, the snowman doll still appears bright with the naive

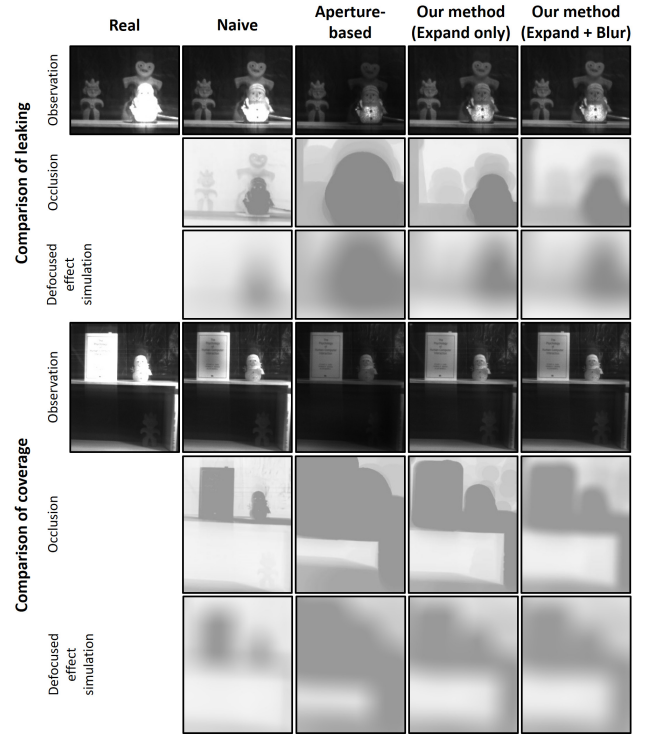


Fig. 9. The real-time observation results with naive mask, aperture-based expansion mask, and proposed masks. Below each mask is the corresponding effect after the out-of-focus simulation.

mask. Conversely, the aperture-based expansion mask must be significantly enlarged to block all incident light at a distance, resulting in an occlusion leak and even occluding the clay statues behind it. When we changed the backdrop color to a lighter tone, the leak effect became more apparent (as shown in Fig. 8). To avoid recomputing the mask, we first recorded the corresponding mask and then statically displayed it on the LCD prior to changing the backdrop.

The results indicate that our image-level optimization strategy results in minimal occlusion leak while maintaining a balanced image contrast. In the second set of comparative studies, we used a reference with regular edges to evaluate mask coverage. The findings show that our approach can achieve more comprehensive masking, even with blurry edges.

C. Additional Blurring Process

We also explored the addition of a pillbox blurring process following the expansion in an effort to soften the mask edges and thereby enhance the masking effect. According to the values derived from the optimization algorithm, the extreme value following the addition of the blurring process is higher than that of the simple expansion (as indicated by the blue curve in Fig. 7(b)). Nonetheless, the advantage of this adjustment is not notably significant, as shown by the rightmost column in Fig. 9.

Following this, we compared the surface plots under both methods. Taking into account the calibration deviations that commonly occur in everyday use (as shown in Fig. 10), a mask with a blurred edge proves more effective at blocking

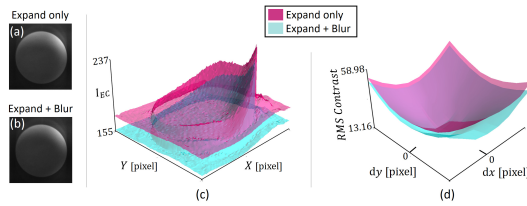


Fig. 10. (a), (b) Experiment under calibration deviation with two proposed masks. (c) The surface plot of the corresponding occluding effect. (d) RMS contrast comparison of two proposed methods at varying degrees of calibration deviation. The X-axis and Y-axis indicate the deviation direction.

incident light at the edges. Calculation of the RMS contrast demonstrates that the extra blur further diminishes the scene contrast, as shown in Fig. 10(d).

VI. DISCUSSION AND FUTURE WORK

We have demonstrated a smart dimming sunglasses system that allows real-time light modulation and balanced scene contrast to alleviate the photophobic effect. In this section, we discuss some objective hardware limitations, and features that have yet to be completed.

a) LCD panel: Since the transparent LCD has to operate with the linear polarizer, the lack of light transmission of LCD has become a clichéd concern. Only 10% of the light transmission is left in the end, as described in Section IV-A. In terms of actual perception, it's similar to the effect of conventional sunglasses when the ambient light is not too strong. A polarizer-free liquid crystal dimmer with 70% transmittance has recently been created as the light dimmer for AR displays [25]. Although it cannot be modulated at the pixel level at present time, the arrival of this device offers us optimism.

b) Eye tracking: The lightweight wearable sunglasses are easy to manufacture given the limited main components. Meanwhile, to manufacture the wearable type, eye-tracking is an essential feature. The user's pupil position is determined to shift the occlusion mask properly. To calculate and evaluate the projective transformation from the real scene to the observed scene, multiple homography matrices can be computed based on a camera system. Then, a real-time calibration between the user's eye and occlusion mask will be performed via a mapping from the camera to the user's eye.

c) User study: While acknowledging that a user study is crucial for confirming the effectiveness of the entire system, we have taken initial steps to verify the essential functions of the system with limited participant testing. We have specifically examined the pupillary light reflex, which is known to occur in individuals with photophobia as well as those without. This examination serves as a preliminary indicator that the system holds promise for individuals with normal vision as well. To further investigate and quantify the system's performance, we plan to conduct a more comprehensive psychophysical experiment in the next phase of our research. This experiment will involve a direct comparison between the proposed mask, conventional naive masks, and aperture-based masks. By conducting a rigorous quantitative analysis, we aim

to provide further evidence of the effectiveness and advantages of our proposed mask over existing alternatives.

VII. CONCLUSIONS

AR and AO technologies are gradually being employed to assist or treat eye disorders as research progresses. To alleviate the photophobic effect, we developed a smart dimming sunglasses system in this paper. While traditional sunglasses and existing global dimming eyeglasses have limitations in complex environments, our smart dimming system utilizes an SLM, a technology commonly used in AR HMDs, to achieve flexible light modulation, in conjunction with a camera for scene detection. We designed a modulation method to cater to the visual needs of photophobic individuals, ensuring they can see in the dark without being overwhelmed by intense light, while still being able to differentiate between light and darkness. Additionally, we presented an optimization strategy to address the issue of a blurry occlusion mask, which arises when the SLM plane is not on the focal plane. Compared to the non-processed mask and the aperture-based expanded mask, the observational results with optimized masks demonstrated more effective modulation.

REFERENCES

- [1] Christa J. Anderson and John Colombo. Larger tonic pupil size in young children with autism spectrum disorder. *Developmental Psychobiology*, 51(2):207–211, 2009.
- [2] Augusto Arias and Pablo Artal. Wavefront-shaping-based correction of optically simulated cataracts. *Optica*, 7(1):22, jan 2020.
- [3] Güneş Aydınoğan, Koray Kavaklı, Afsun Şahin, Pablo Artal, and Hakan Ürey. Applications of augmented reality in ophthalmology. *Biomedical optics express*, 12(1):511–538, 2021.
- [4] Margaret L Bauman and Thomas L Kemper. Neuroanatomic observations of the brain in autism: a review and future directions. *International journal of developmental neuroscience*, 23(2-3):183–187, 2005.
- [5] Rami Burstein, Rodrigo Nosedá, and Anne B. Fulton. Neurobiology of Photophobia. *Journal of Neuro-Ophthalmology*, 39(1):94–102, 2019.
- [6] Joseph Clark, Kimberly Hasselfeld, Kathryn Bigsby, and Jon Divine. Colored Glasses to Mitigate Photophobia Symptoms Posttraumatic Brain Injury. *Journal of Athletic Training*, 52(8):725–729, 2017.
- [7] Xiaofei Fan, Judith H. Miles, Nicole Takahashi, and Gang Yao. Abnormal transient pupillary light reflex in individuals with autism spectrum disorders. *Journal of Autism and Developmental Disorders*, 39(11):1499–1508, 2009.
- [8] PA Good, RH Taylor, and MJ Mortimer. The use of tinted glasses in childhood migraine. *Headache: The Journal of Head and Face Pain*, 31(8):533–536, 1991.
- [9] Joseph W Goodman. *Introduction to Fourier optics*. Roberts and Company publishers, 2005.
- [10] N Hasan, M Karkhanis, C Ghosh, F Khan, Tridib Ghosh, Hanseup Kim, and CH Mastrangelo. Lightweight smart autofocusing eyeglasses. In *MOEMS and Miniaturized Systems XVII*, volume 10545, pages 26–31. SPIE, 2018.
- [11] Nazmul Hasan, Mohit Karkhanis, Fariha Khan, Tridib Ghosh, Hanseup Kim, and Carlos H. Mastrangelo. Adaptive optics for autofocusing eyeglasses. *Optics InfoBase Conference Papers*, Part F45-I(January):1–4, 2017.
- [12] Yuichi Hiroi, Yuta Itoh, Takumi Hamasaki, and Maki Sugimoto. Advisor: Assisting eye adaptation via occlusive optical see-through head-mounted displays. In *Proceedings of the 8th Augmented Human International Conference*, pages 1–9, 2017.
- [13] Xiaodan Hu, Yan Zhang, Naoya Isoyama, Nobuchika Sakata, and Kiyoshi Kiyokawa. Design and prototyping of computational sunglasses for autism spectrum disorders. In *Proceedings - 2021 IEEE Conference on Virtual Reality and 3D User Interfaces Abstracts and Workshops, VRW 2021*, pages 581–582, 2021.

- [14] Yuta Itoh, Takumi Hamasaki, and Maki Sugimoto. Occlusion Leak Compensation for Optical See-Through Displays Using a Single-Layer Transmissive Spatial Light Modulator. *IEEE Transactions on Visualization and Computer Graphics*, 23(11):2463–2473, 2017.
- [15] Bradley J. Katz and Kathleen B. Digre. Diagnosis, pathophysiology, and treatment of photophobia. *Survey of Ophthalmology*, 61(4):466–477, 2016.
- [16] K. Kiyokawa, M. Billinghamurst, B. Campbell, and E. Woods. An occlusion capable optical see-through head mount display for supporting co-located collaboration. In *Proceedings of the Second IEEE and ACM International Symposium on Mixed and Augmented Reality, 2003*, pages 133–141, 2003.
- [17] Tobias Langlotz, Jonathan Sutton, Stefanie Zollmann, Yuta Itoh, and Holger Regenbrecht. Chromaglasses: Computational glasses for compensating colour blindness. In *Proceedings of the 2018 CHI Conference on Human Factors in Computing Systems*, pages 1–12, 2018.
- [18] J. E. Lebensohn and John Bellows. The nature of photophobia. *Archives of Ophthalmology*, 12(3):380–390, 1934.
- [19] Andrew Maimone and Henry Fuchs. Computational augmented reality eyeglasses. In *2013 IEEE International Symposium on Mixed and Augmented Reality, ISMAR 2013*, pages 29–38, 2013.
- [20] Alan Main, Ioannis Vlachonikolis, and Andrew Dowson. The wavelength of light causing photophobia in migraine and tension-type headache between attacks. *Headache: The Journal of Head and Face Pain*, 40(3):194–199, 2000.
- [21] Merriam-Webster. Photophobia, 2021.
- [22] Shree K. Nayar and Vlad Branzoi. Adaptive dynamic range imaging: Optical control of pixel exposures over space and time. In *Proceedings of the IEEE International Conference on Computer Vision*, volume 2, pages 1168–1175, 2003.
- [23] Nitish Padmanaban, Robert Konrad, and Gordon Wetzstein. Autofocals: Evaluating gaze-contingent eyeglasses for presbyopes. *Science Advances*, 5(6):eaav6187, jun 2019.
- [24] Bahman Taheri, Tamas Kosa, Christine Baker, and Volodymyr Bodnar. Variable light attenuating devices and arrangements, jun 2019. US Patent 10,310,349.
- [25] Javed Rouf Talukder, Hung-Yuan Lin, and Shin-Tson Wu. Photo- and electrical-responsive liquid crystal smart dimmer for augmented reality displays. *Optics Express*, 27(13):18169, 2019.
- [26] Arnaud JP Vincent, Egilius LH Spierings, and Harley B Messinger. A controlled study of visual symptoms and eye strain factors in chronic headache. *Headache: The Journal of Head and Face Pain*, 29(8):523–527, 1989.
- [27] Gordon Wetzstein, Wolfgang Heidrich, and David Luebke. Optical image processing using light modulation displays. *Computer Graphics Forum*, 29(6):1934–1944, 2010.
- [28] World Health Organization. Vision impairment and blindness, 2022.
- [29] Yan Zhang, Xiaodan Hu, Kiyoshi Kiyokawa, Naoya Isoyama, Nobuchika Sakata, and Hong Hua. Optical see-through augmented reality displays with wide field of view and hard-edge occlusion by using paired conical reflectors. *Optics letters*, 46(17):4208–4211, 2021.
- [30] Yan Zhang, Xiaodan Hu, Kiyoshi Kiyokawa, Naoya Isoyama, Hideaki Uchiyama, and Hong Hua. Realizing mutual occlusion in a wide field-of-view for optical see-through augmented reality displays based on a paired-ellipsoidal-mirror structure. *Optics Express*, 29(26):42751–42761, 2021.